

Article

The Application of Sulfur–Metal Mass Ratios in Metal Sulfides in Assessing Prospects for Deep Metallogeny: A Case Study of the Tongshan Copper Deposit in Heilongjiang Province, Northeast China

Ruixuan Lan ^{1,2}, Lixin Zhu ³, Shixin Tang ¹, Zhuang Duan ¹, Yong Li ¹ and Shengming Ma ^{1,*}

¹ Institute of Geophysical and Geochemical Exploration, Chinese Academy of Geological Sciences, Langfang 065000, China; lanruixuan@email.cugb.edu.cn (R.L.); tshixin@mail.cgs.gov.cn (S.T.); zduan_geology@163.com (Z.D.); cgslyong@mail.cgs.gov.cn (Y.L.)

² Chinese Academy of Geological Sciences, China University of Geosciences, Beijing 100083, China

³ Development Research Centre, China Geological Survey, Beijing 100037, China; lixinz@cags.ac.cn

* Correspondence: msmigge@163.com

Abstract: Sulfur–metal mass ratios (SMMRs) between sulfur and metal elements (Cu, Pb, Zn, Ag, Fe, etc.) in metal sulfides are fixed in idealized compositions, so they should have a relatively fixed proportion in terms of mass without considering the presence of structural defects such as vacancies or substitution elements. Rock bodies with an SMMR of S far greater than the common metal sulfides may contain additional sulfides of other metals. We studied the Tongshan copper deposit in NE China and calculated the mass transfer of various elements in drill hole ZK611 samples. The data show a S influx of 7160 g/t, a Cu influx of 5469 g/t, and an Fe influx of 8796 g/t in the Cu ore body. Below the Cu ores, the average influx is 18,600 g/t of S, 650 g/t of Cu, and 5360 g/t of Fe, which provides an SMMR far above common mineral sulfide values. Further studies indicated that this rock unit contains fine-grained sphalerite and galenite, and when Zn and Pb are included in the rock SMMR calculations, values closer to the mineral sulfides emerge. These results imply that the coordinating balance relationship of S content with Fe and other ore-forming metals could provide direct information for assessing metallogenic prospects.

Keywords: sulfur–metal mass ratios; element migration quantity; the Tongshan copper deposit; evaluation of deep metallogenic prospects



Citation: Lan, R.; Zhu, L.; Tang, S.; Duan, Z.; Li, Y.; Ma, S. The Application of Sulfur–Metal Mass Ratios in Metal Sulfides in Assessing Prospects for Deep Metallogeny: A Case Study of the Tongshan Copper Deposit in Heilongjiang Province, Northeast China. *Minerals* **2024**, *14*, 1069. <https://doi.org/10.3390/min14111069>

Academic Editor: Paul Alexandre

Received: 4 June 2024

Revised: 8 October 2024

Accepted: 17 October 2024

Published: 24 October 2024



Copyright: © 2024 by the authors. Licensee MDPI, Basel, Switzerland. This article is an open access article distributed under the terms and conditions of the Creative Commons Attribution (CC BY) license (<https://creativecommons.org/licenses/by/4.0/>).

1. Introduction

Geochemical exploration is an indispensable tool for prospecting endogenous non-ferrous and noble metal deposits and has played a critical role in mineral exploration at varying scales [1,2]. In recent decades, geochemical exploration techniques have made great progress [3,4], and the advancement of analytical techniques [5], improvements in geochemical data interpretation [6], and the use of 3D geochemical-visualizing techniques [7] have strongly supported the acquisition and presentation of geochemical information. However, the shift of prospecting work from shallow to deep presents a new challenge for these techniques, and there are still some aspects to be explored and improved [8]. As it should be, this is also a hard-won development opportunity for geochemical exploration.

In exploration areas using drilling engineering, the question of how to further evaluate metallogenic prospects is of significant importance for delineating prospecting targets, prospecting work deployment, and achieving prospecting breakthroughs, so it is urgent to find an effective solution. Geochemical exploration techniques are a valuable tool, but they provide a paucity of metallogenic information at this stage. The currently utilized univocal geochemical exploration indices, unable to provide abundant information, may contribute to this issue. Therefore, based on 30 known deposits and mineral exploration areas,

this study integrates geochemical anomalies of distinct attributes and their implications in metallogenic systems [9–13], proposes a new idea for a multi-dimensional anomaly system [14], and emphasizes the importance of the metallogenic indication of mineralizing agents represented by sulfur anomalies [15].

The element sulfur, a typical chalcophile and mineralizing agent, is indispensable for the ore-forming materials of most non-ferrous metal deposits. In ore-forming processes, the element sulfur combines with various metal elements to form metal sulfides due to its chalcophile properties. Therefore, we can use the synergistic relationship of sulfur anomalies with Fe and other ore-forming elements to judge whether mineralization stops, as well as the mineralization possibility of deep and peripheral areas. Sulfur anomaly is a kind of geochemical anomaly, which means the content of sulfur in the wall rock or geological body is higher than its background value or Clark value (260 ppm, Taylor (1964) [16]). It is mainly assessed in the primary halo study of a drill hole; if sulfur in the core sample is high (an extremely significant positive anomaly), it suggests good metallogenic potential in the area passed through by the drill hole. However, if the sulfur content is low (a weak positive anomaly), this area would develop an ore body with a lower metallogenic potential. Furthermore, many ore geologists believe that sulfur is a major component in magmatic–hydrothermal ores, including porphyry copper, skarn, and polymetallic vein deposits, where it is enriched to a greater degree than any of the ore metals themselves [17]. Individual porphyry copper deposits are crustal sulfur anomalies, commonly exceeding one billion tons of sulfur [18].

For any given metal sulfide mineral, there is a fixed sulfur–metal mass ratio between sulfur and the metal elements, which is the basis for applying a sulfur anomaly to mineralization intensity and metallogenic prospect evaluation. However, little attention has been paid to this aspect. This study enriches and improves the application of sulfur–metal mass ratios (SMMRs) of sulfur to metal elements in metal sulfides for metallogenic prospect evaluation and further validates their practical value through test results. The SMMR is calculated as $S/(S+\text{metals of interest})$, for example, $S/(S + \text{Cu} + \text{Fe})$ for chalcopyrite, and not as $S/(\text{Fe} + \text{Cu})$; $S/(S + \text{Fe})$ for pyrite, and not as S/Fe .

1.1. Geochemical Features of Sulfur

Sulfur (S), in the third period in the sixth group of the periodic table, is a typical nonmetal element [19]. Sulfides rank second in their number, followed by oxides, in nature. Most elements that combine with S are called chalcophile elements, including about 40 kinds of elements, and these can be further divided into nonmetal and metal elements; these kinds of metal elements are dominated by the siderophile element Fe. Other elements that can combine with S to form common compounds include Zn, Pb, Cu, Ag, Sb, Bi, Ni, Co, Mo, Hg, etc. The combination of H with S exerts a key role in the formation of metal sulfides. Sulfur-bearing minerals in the Earth's crust include sulfides of the sulfur complex, sulfate salts, and sulfosalts. Sulfur combines with various elements in different valences under contrasting oxidation conditions and shows a varying trend with increasing oxidation.

Most sulfides are stable under reduced conditions and will oxidize in supergene conditions. In the sulfide oxidation processes, bacteria and electrochemical processes attract much attention besides the above geochemical features of S [20–22]. The oxidation of S leads to considerable S leaching, resulting in a weakening metallogenic indication of S. However, this also changes the supergene environments of mineralized sections, which may lead to the derivation of other feasible geochemical exploration methods [23].

The above geochemical features of S emphasize its dominant role in forming minerals and sulfide deposits [24–29]. S is a mineralizing agent for transporting ore materials and is also an important component of sulfide. This also highlights the role of S in geochemical exploration. Therefore, the SMMR of S with other ore-forming elements in metal sulfide minerals and S anomaly in rocks can be used to evaluate the mineralization possibility of metal elements and thus predict the metallogenic prospects.

1.2. Sulfur–Metal Mass Ratios of Common Metal Sulfide Minerals

Most ore-forming minerals of non-ferrous metal deposits are metal sulfide minerals. Ore-forming minerals for different deposits are distinct in ore-forming elements and associated elements but are similar in S. Table 1 lists some metal elements and metal sulfide minerals that can combine with S to form common compounds. It indicates that these metal sulfide minerals always contain S. The SMMR for some metal sulfide minerals based on the crystal chemical formula of common compounds is also shown in Table 1. It implies that the SMMR of S is the largest (35.0 wt.%) for chalcopyrite among copper-bearing sulfide minerals, while that for chalcocite is the smallest (only 20.1 wt.%). The SMMR for lead-bearing sulfide minerals is commonly small; the highest is found for jamesonite (23.1 wt.%), and the smallest is found for galena (13.4 wt.%). The SMMRs of S for sphalerite and wurtzite are generally the same (32.9 wt.%). Argentite contains 12.9 wt.% S, ranking the lowest in our statistical results, and pyrite contains 53.4 wt.% S, ranking the highest in our statistical results. Pyrrhotite contains 39 wt.%–40 wt.% S. The metal sulfide minerals listed in Table 1 are the common major ore-forming minerals for corresponding metal deposits, implying that S is essential for the formation of non-ferrous metal deposits and that the S content and S anomaly can be utilized to predict metallogenic prospects.

Table 1. Sulfur–metal mass ratios in common metal sulfide and sulfosalt minerals.

Element	Mineral	Formula	Sulfur–Metal Mass Ratio (wt.%)		
Cu	Chalcopyrite	CuFeS ₂	Cu34.6	Fe30.4	S35.0
	Bornite	Cu ₅ FeS ₄	Cu63.3	Fe11.1	S25.6
	Tetrahedrite-(Cu)	Cu ₁₂ Sb ₄ S ₁₃	Cu45.9	Sb29.2	S24.9
	Chalcocite	Cu ₂ S	Cu79.9		S20.1
	Covellite	CuS	Cu66.5		S33.5
Pb	Galena	PbS	Pb86.6		S13.4
	Jamesonite	Pb ₄ FeSb ₆ S ₁₄	Pb40.1	Fe2.7, Sb35.5	S21.7
	Bourbonite	PbCuSbS ₃	Pb42.4	Cu13.0, Sb24.9	S19.7
Zn	Sphalerite	ZnS	Zn67.1		S32.9
	Wurtzite	ZnS	Zn67.1		S32.9
Ag	Argentite	Ag ₂ S	Ag87.1		S12.9
Fe	Pyrite	FeS ₂	Fe46.6		S53.4
	Pyrrhotite	Fe _{1-x} S	Fe61-60		S39-40

The SMMR of metal sulfide minerals indicates that S anomaly has a closely positive relationship with non-ferrous mineralization intensity. The stronger the mineralization is, the more obvious the S anomaly, but conversely, if the S anomaly is obviously strong, mineralization may be weak. This is the key technical problem encountered when using a S anomaly to predict metallogenic prospects. In nature, S is more prone to combine with Fe to form pyrite or pyrrhotite than other metal elements such as Cu, Pb, and Zn. The element S occupies a high proportion in pyrite or pyrrhotite. Therefore, if Fe is in a metallogenic system, the combination of Cu, Pb, and Zn with S is constrained, and so is the mineralization. Hence, when the S anomaly is used to evaluate metallogenic prospects, the synergistic balance relationship between S and Fe and other ore elements should also be considered. In addition, the extent to which the S anomaly can forecast mineralization is also associated with certain mineral species. For instance, in a single Cu or Ag ore deposit, the content of S is highly variable, which is interpreted to depend on the high variations of Cu and Ag abundant in the crust (a three-order difference in magnitude) and a lower SMMR of S in Ag-bearing mineral (argentite) than that in Cu-bearing mineral (chalcopyrite).

Thus, S anomaly is utilized in two aspects: if metallogeny occurs in the prospects, and if the potential of metallogeny in the deep exists. In the following section, we will

discuss these aspects while using the Tongshan copper deposit in Heilongjiang province as an example.

2. Geological Setting

2.1. Duobaoshan Ore Field

The Duobaoshan ore field is situated in Heilongjiang Province, China, on the eastern side of the Central Asian Orogenic Belt (CAOB), to the west of the Hegenshan–Heihe suture zone, which divides the Xing’an and Songnen blocks [30–32]. Multiple terrane collisions have characterized the tectonic evolution of the Xing’an–Mongolia Orogenic Belt in the Phanerozoic era (Figure 1a). The northeast section of the belt is fragmented into four blocks by the Tayuan–Xiguitu, Hegenshan–Heihe, and Mudanjiang fault zones [33–36]. From northwest to southeast, these four blocks are Ergun, Xing’an, Songnen, and Jiamusi [37]. Since the Early Paleozoic, the Ergun Block has remained stable [38]. In the Middle Paleozoic, the Xing’an Block gathered along the Tayuan–Xiguitu fault toward the Ergun Block [39,40]. In the Late Paleozoic, along the Hegenshan–Heihe fault, the Songnen Block collided with the Xing’an Block and Ergun Block [41]. In the Early Mesozoic, along the Mudanjiang fault, the Jiamusi Block also collided with the Xing’an Block and Ergun Block [42]. The Duobaoshan ore field is located in the Xing’an Block in the northwest of the Hegenshan–Heihe fault. The strata in this area are mainly Ordovician and Silurian, followed by Devonian and Cretaceous (Figure 1b). The main ore-bearing strata are the Tongshan formation and the Duobaoshan formation. The former is composed of tuffaceous sandstone, siltstone, tuff, and crystalline limestone, while the latter is composed of andesite, dacite, and pyroclastic rock, with interbedded marble and slate [43–45].

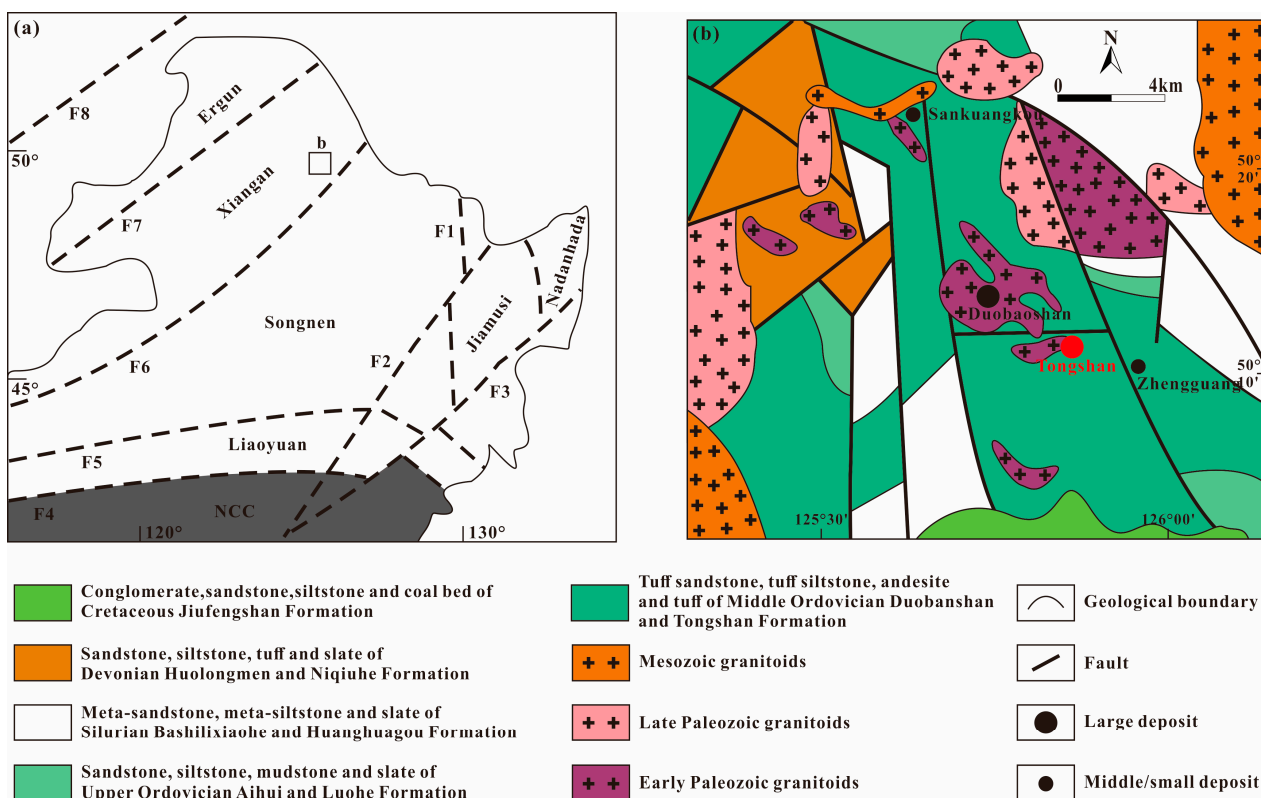


Figure 1. (a) A sketch tectonic map of the Xing’an–Mongolia orogenic belt (modified from [30]); (b) a simplified geological map of the Duobaoshan ore field (modified from [37]). In (a), F1 represents the Mudanjiang fault, F2 represents the Yitong–Yilan fault, F3 represents the Dunhua–Mishan fault, F4 represents the Chifeng–Kaiyuan fault, F5 represents the Xilamulun–Changchun fault, F6 represents the Hegenshan–Heihe fault, F7 represents the Tayuan–Xiguitu fault, and F8 represents the Mongolia–Okhotsk fault.

2.2. Tongshan Copper Deposit

The Tongshan copper deposit is sited in the northeastern segment of the Daxinganling fold system, and the middle part of the NW-trending tectonomagmatic belt northwest of the Xinkailing deep fault. The outcropped strata are the Middle Ordovician Tongshan formation (O_2t) and Duobaoshan formation (O_2d) (Figure 2). The Tongshan formation is composed of intermediate acidic tuff, dacite, and quartz sandstone, and the Duobaoshan formation is dominated by andesite and intermediate acidic tuff acting as country rocks of the Tongshan deposit [46]. The country rock alteration is chiefly potassic silicification, phyllic alteration, and propylitization, and orebodies mainly occur in the phyllic alteration belts. Intrusive rocks include the Middle Hercynian granodiorite ($\gamma\delta_4^2$) and Late Hercynian trondhjemite ($\gamma\delta_4^3$). Isotopic dating suggests that the mineralization principally occurred in the Late Hercynian to Indosinian. Re-Os isotopic dating indicates that ore materials may derive from the Late Ordovician, migrating from country rocks [47], and are enriched in favorable positions such as extensional structures [48]. Fluid inclusion studies indicate that the ore-forming fluids in the Tongshan deposit experienced three stages, and fluid boiling resulting from the decrease in pressure is the major mechanism for the precipitation of chalcopyrite [49].

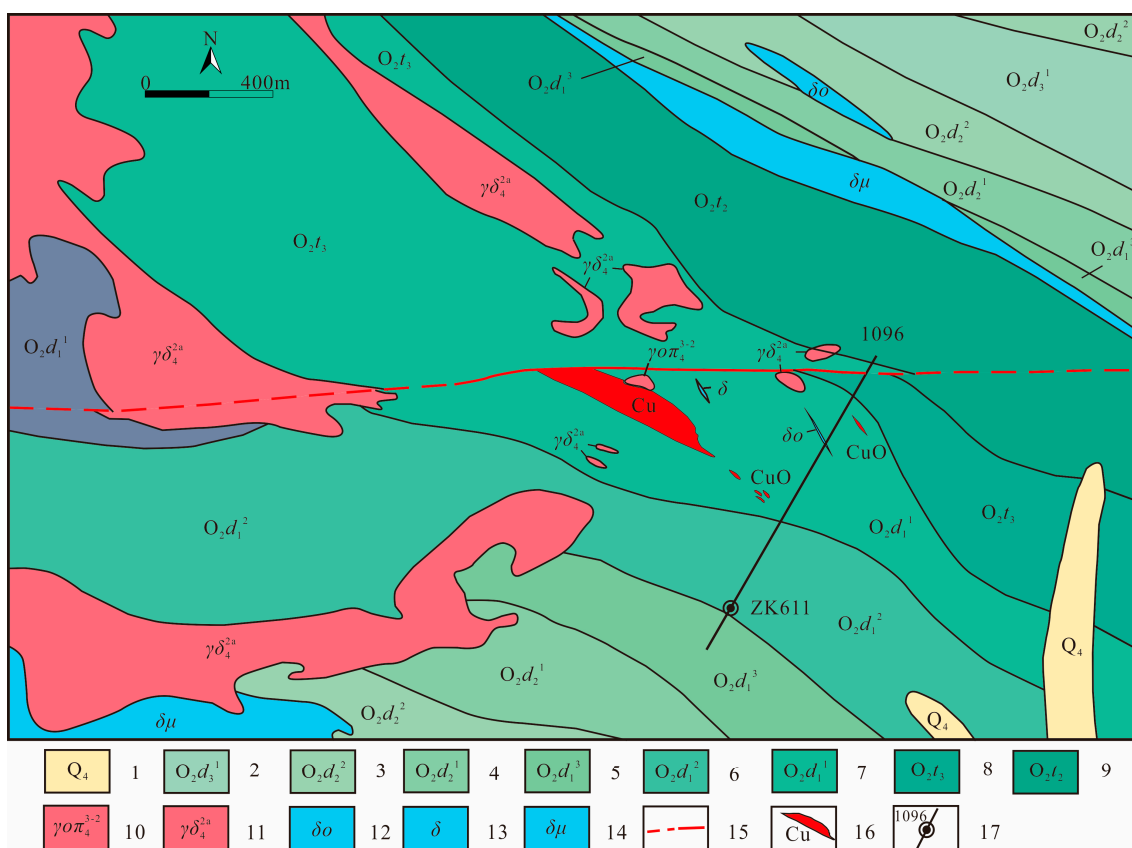


Figure 2. Simplified geological map of the Tongshan copper deposit (modified from [15]). 1—Quaternary; 2—Middle Ordovician Duobaoshan formation, 3rd member, 1st submember; 3—Middle Ordovician Duobaoshan formation, 2nd member, 2nd submember; 4—Middle Ordovician Duobaoshan formation, 2nd member, 1st submember; 5—Middle Ordovician Duobaoshan formation, 1st member, 3rd submember; 6—Middle Ordovician Duobaoshan formation, 1st member, 2nd submember; 7—Middle Ordovician Duobaoshan formation, 1st member, 1st submember; 8—Middle Ordovician Tongshan formation, 3rd member; 9—Middle Ordovician Tongshan formation, 2nd member; 10—Plagioclase granite porphyry; 11—Granodiorite; 12—Quartz diorite; 13—Diorite; 14—Diorite porphyry; 15—Inferred and measured fault; 16—Copper orebody; 17—Exploration line and drill hole.

3. Experimental Research Methods

3.1. Sample Collection

Samples from the Tongshan copper deposit were collected from drill ZK611 cores. Overall, 56 samples were collected from this hole with a depth of 604 m, and the sampling interval was 5–8 m. Within every sampling interval, we collected samples by continuously picking rock blocks, and 8–10 pieces of 20–30 g weight rock samples comprised an analytical sample with a total weight of 200–300 g. In addition, samples within a sample interval are generally the same in rock lithology, alteration, and mineralization so that the adequate representation of rocks is achieved.

3.2. Sample Processing and Analysis

Rock samples were processed through three steps of crushing. First, the samples were coarsely crushed to <3–5 mm with a jaw crusher, the jaw plate material of which is high-aluminum porcelain, then ground to <0.9 mm (20 mesh) with a disc crusher, and then ground to <0.074 mm (200 mesh) with an agate ball mill. These procedures were strictly controlled in order to avoid sample contamination and pollution.

The samples were then analyzed in the central laboratory of the Institute of Geophysical and Geochemical Exploration, CAGS. The analytical methods and detection limit are listed in Table 2. The quality control of sample analysis adopted standard substance and repeated samples, and the results show that the passing rate was 100%.

Table 2. Sample analysis methods and quality monitoring results.

Analytical Items	Analytical Methods	Detection Limit	Unit	Passing Rate of One-Order Standard Material/%	Passing Rate of Repeated Samples/%
S	WD-XRF	50	ppm	100	100
Cu	ICP-MS	1	ppm	100	100
Pb	ICP-MS	2	ppm	100	100
Zn	ICP-MS	2	ppm	100	100
Ag	A.C.-Arc-SES	20	ppb	100	100
Fe ₂ O ₃	WD-XRF	0.1	wt.%	100	100

Note: WD-XRF = Wavelength Dispersive X-Ray Fluorescence Spectrometry; ICP-MS = Inductively Coupled Plasma Mass Spectrometry; A.C.-Arc-SES = Alternating Current Arc Source Emission Spectrometry.

3.3. Calculation of Element Migration

The SMMR of S with metal elements is a good method used to predict metallogenic prospects; these ratios are those of element migration quality between S and ore-forming elements, which are based on element flux. However, only the element content is available currently. This poses a difficult problem: using the element content to estimate its mass migration, i.e., the element influx, element efflux, and their mass. Only by solving this problem can we further discuss the SMMR between S and ore-forming elements and thus use the S anomaly to evaluate the metallogenic prospects of a mineral exploration area.

This problem stems from studying the mass balance of the geochemical open system category. Since the 1970s, many researchers have discussed this issue and achieved fruitful results, of which the Gresens equation deduced by Gresens (1967) [50] created a new situation of using rock analytical data in rock mass balance. On this basis, Grant (1986) [51] proposed the concentration line method (isocon), greatly simplifying the mass balance calculation, and achieved a widespread application in hydrothermal alteration and migmatization [52]. Deng et al. (1999) [53] derived two new expressions based on the Grant equation to discuss the quality changes and quality change rates of active elements.

This paper utilizes Grant's concentration line equation to discuss the SMMR of S with metallogenic elements.

$$\Delta C_i = (M^A/M^O)C_i^A - C_i^O = (C_j^O/C_j^A)C_i^A - C_i^O$$

where ΔC_i is the migration quantity of element i , M^A is the mass of altered rocks, M^O is the mass of original rocks, C_i^A is the content of element i in altered rocks, C_i^O is the content of element i in original rocks, C_j^O is the inert element j in original rocks, and C_j^A is the content of inert element j in altered rocks. According to previous studies [54–56], Al_2O_3 is usually immobile in mass transfer [57–60], so we selected Al_2O_3 as an inert element, and j in the equation is Al_2O_3 , with i representing S, Fe, Cu, Pb, Zn, and Ag.

In calculating element migration quantity, the element content of original rocks for altered rocks is also needed, as opposed to mineralized or altered rocks. However, due to the widespread alteration and mineralization and varying types of rocks, unaltered original rocks were unobtainable in this study. Considering this point and integrating information from experimental studies, this study adopted different methods to ascertain the element content in original rocks. The background content of inert Al_2O_3 and major Fe uses the median content of Al_2O_3 and Fe for every drill core; the background values of S, Cu, Pb, Zn, and Ag in the Tongshan copper deposit adopt the chemical composition of andesite pyroclastic rocks, andesite, and sandstone in East China [61].

For most rock samples, this study only describes the element migration quantity for every drill hole based on the same lithology or mineralization type. Thus, the merged statistical results are based on lithology or mineralization types.

3.4. Steps and General Rules for Evaluation of Metallogenic Prospects Using Sulfur–Metal Mass Ratios

1. Based on Grant's concentration equation and element content in altered rocks, this study used Al_2O_3 as the inert (immobile) element and calculated the element migration quantity of S, Cu, Pb, Zn, As, and Ag in the geochemical systems of the test areas. We obtained the content of Fe_2O_3 via sample analysis, so the content of Fe can be obtained using $Fe = 112 \times Fe_2O_3 / 160$. Furthermore, the element migration quantity of Fe can be obtained using Grant's concentration equation.
2. The element migration quantity and variations of S can be used preliminarily to judge whether there were hydrothermal processes or mineralization in drillholes, the overall mineralization intensity, and the possible mineralization sections.
3. On the premise that mineralization is judged to exist, differing element migration of S and Fe can be used to interpret element migration and S content and further to judge whether there are metallogenic conditions for forming non-ferrous metal deposits.
4. On the premise that non-ferrous metal deposits or mineralization are inferred to exist, the element migration quantity of metallogenic elements can be utilized to infer possible mineral species. Then, the identification of polished sections was performed to ensure the mineralization process and thus discover mineralization.
5. If there are good metallogenic prospects in deep or peripheral areas, exploration or prospecting engineering should be deployed to validate this.
6. When using the S anomaly to evaluate the metallogenic prospects of an exploration area, the above steps and general rules are generally progressive. Usually, if the previous condition does not exist, the following step will terminate.

4. Result

The element concentrations of S, Fe, Cu, Pb, Zn, and Ag in drill hole ZK611 in the Tongshan copper deposit are listed in Table 3. The element migration quantity of S, Fe, Cu, Pb, Zn, and Ag in the Tongshan copper deposit is calculated and listed in Table 4 in the order of lithology. The element flux of S, Fe, Cu, Pb, Zn and Ag of each sample is shown in Table 5. Generally, the S in drill hole ZK611 shows an influx feature, which provides material for mineralization, but its influx degree varies greatly. In the sections of andesite tuff at a depth of 0–272 m and andesite at a depth of 272–400 m, the influx of S is small, averaging less than 1000 g/t; in altered andesite at a depth of 400–494 m, the influx of S becomes larger, corresponding to the appearance of chalcopyrite; in the section with chloritization, sericitization, and weak copper mineralization of andesite, the influx of S

appears as the greatest, averaging 18,575 g/t, which is in disagreement with the weak copper mineralization. In sandstone below the altered andesite, the influx of S is 1432 g/t, which shows an influx characteristic. However, the S influx dramatically decreased relative to the overlying andesite. It is suggested that the S influx does not closely correspond to the copper mineralization intensity. In the chloritized and sericitized andesite sections (494–581 m) with the largest S influx, the influx of Cu averages only 652 g/t, while in the copper mineralized andesite section (400–494 m) with the largest Cu influx, the S influx is 7160 g/t, about 39% of the largest S influx.

Table 3. The element contents (S, Fe, Cu, Pb, Zn, and Ag) of samples from the ZK611 drill hole.

Sample Number	Location/m	S/ppm	Fe/wt.%	Cu/ppm	Pb/ppm	Zn/ppm	Ag/ppb
ZK611-1	28	223	5.96	120	17	191	883
ZK611-2	50	2899	4.70	162	288	1365	1669
ZK611-3	69	411	6.36	190	132	386	1095
ZK611-4	90	2231	6.87	157	58	1936	1187
ZK611-5	96	537	6.07	304	28	168	274
ZK611-6	121	168	6.75	155	5	102	445
ZK611-7	140	292	6.13	117	13	187	345
ZK611-8	155	231	7.78	281	10	124	359
ZK611-9	170	380	7.55	185	12	121	186
ZK611-10	191	142	7.79	178	17	109	383
ZK611-11	211	340	8.27	254	26	142	538
ZK611-12	230	1539	6.65	633	54	265	1825
ZK611-13	251	358	4.32	134	212	157	439
ZK611-14	263	185	6.69	149	20	105	282
ZK611-15	272	127	6.59	129	7	103	210
ZK611-16	281	212	5.84	208	119	135	911
ZK611-17	288	85	4.40	64	15	96	138
ZK611-18	300	110	5.96	97	6	94	153
ZK611-19	311	485	5.64	105	24	382	545
ZK611-20	320	152	5.67	80	15	124	121
ZK611-21	329	284	5.15	104	13	100	160
ZK611-22	341	114	3.64	65	9	143	86
ZK611-23	350	1528	7.16	262	23	211	382
ZK611-24	362	8349	6.68	772	45	96	1447
ZK611-25	371	568	5.36	183	14	131	163
ZK611-26	379	635	4.68	108	30	144	244
ZK611-27	388	391	5.64	133	104	230	512
ZK611-28	400	124	4.88	42	30	173	232
ZK611-29	413	10,905	7.50	5522	63	154	9569
ZK611-30	421	2756	5.86	2189	4	52	1390
ZK611-31	430	6248	6.46	5545	4	51	2576
ZK611-32	440	7867	5.64	4400	12	75	2337
ZK611-33	449	2794	4.87	2318	6	62	1183
ZK611-34	458	8340	7.63	5472	8	129	3068
ZK611-35	470	17,571	8.53	18,415	43	122	7745
ZK611-36	473	7522	6.28	7011	10	97	2362
ZK611-37	479	5769	6.80	5650	4	92	1746
ZK611-38	483	9349	7.76	7377	6	97	4405
ZK611-39	488	4769	7.04	1406	7	130	495
ZK611-40	494	5223	7.57	1275	8	192	852
ZK611-41	500	4760	6.13	238	30	3865	782
ZK611-42	506	11,100	6.97	149	411	3006	1396

Table 3. Cont.

Sample Number	Location/m	S/ppm	Fe/wt. %	Cu/ppm	Pb/ppm	Zn/ppm	Ag/ppb
ZK611-1	28	223	5.96	120	17	191	883
ZK611-2	50	2899	4.70	162	288	1365	1669
ZK611-3	69	411	6.36	190	132	386	1095
ZK611-4	90	2231	6.87	157	58	1936	1187
ZK611-5	96	537	6.07	304	28	168	274
ZK611-6	121	168	6.75	155	5	102	445
ZK611-7	140	292	6.13	117	13	187	345
ZK611-8	155	231	7.78	281	10	124	359
ZK611-9	170	380	7.55	185	12	121	186
ZK611-10	191	142	7.79	178	17	109	383
ZK611-11	211	340	8.27	254	26	142	538
ZK611-12	230	1539	6.65	633	54	265	1825
ZK611-13	251	358	4.32	134	212	157	439
ZK611-14	263	185	6.69	149	20	105	282
ZK611-15	272	127	6.59	129	7	103	210
ZK611-16	281	212	5.84	208	119	135	911
ZK611-17	288	85	4.40	64	15	96	138
ZK611-18	300	110	5.96	97	6	94	153
ZK611-19	311	485	5.64	105	24	382	545
ZK611-20	320	152	5.67	80	15	124	121
ZK611-21	329	284	5.15	104	13	100	160
ZK611-22	341	114	3.64	65	9	143	86
ZK611-23	350	1528	7.16	262	23	211	382
ZK611-24	362	8349	6.68	772	45	96	1447
ZK611-25	371	568	5.36	183	14	131	163
ZK611-26	379	635	4.68	108	30	144	244
ZK611-27	388	391	5.64	133	104	230	512
ZK611-28	400	124	4.88	42	30	173	232
ZK611-29	413	10,905	7.50	5522	63	154	9569
ZK611-30	421	2756	5.86	2189	4	52	1390
ZK611-31	430	6248	6.46	5545	4	51	2576
ZK611-32	440	7867	5.64	4400	12	75	2337
ZK611-33	449	2794	4.87	2318	6	62	1183
ZK611-34	458	8340	7.63	5472	8	129	3068
ZK611-35	470	17,571	8.53	18,415	43	122	7745
ZK611-36	473	7522	6.28	7011	10	97	2362
ZK611-37	479	5769	6.80	5650	4	92	1746
ZK611-38	483	9349	7.76	7377	6	97	4405
ZK611-39	488	4769	7.04	1406	7	130	495
ZK611-40	494	5223	7.57	1275	8	192	852
ZK611-41	500	4760	6.13	238	30	3865	782
ZK611-42	506	11,100	6.97	149	411	3006	1396

Table 4. Statistics of the element migration quantity in the ZK611 drill hole.

Layers	Drill Hole Depth (m)	Main Lithology	ΔS	ΔFe	ΔCu	ΔPb	ΔZn	ΔAg
1	0–272	Andesite tuff (15)	695	19,281	201	52	297	0.67
2	272–400	Andesite (13)	803	−2172	133	20	60	0.35
3	400–494	Chalcopyritized andesite (12)	7160	8796	5469	1.0	3.0	3.2
4	494–581	Altered andesite (14)	18,575	5359	652	4653	18,836	8.0
5	581–604	Sandstone (2)	1432	4952	1010	26	193	1.8

Note: positive numbers indicate element influx in the system, and a negative number indicates element efflux. The unit of migration quantity is g/t. Figures in brackets represent the numbers of samples used for statistics.

Table 5. The element flux (S, Fe, Cu, Pb, Zn, and Ag) of samples in the ZK611 drill hole.

Sample Number	Location/m	ΔS (g/t)	ΔFe (g/t)	ΔCu (g/t)	ΔPb (g/t)	ΔZn (g/t)	ΔAg (mg/t)
ZK611-1	28	185	8753	102	−1	98	812
ZK611-2	50	4015	16,844	212	384	1817	2289
ZK611-3	69	390	16,228	180	118	308	1079
ZK611-4	90	1861	9396	119	32	1553	966
ZK611-5	96	601	22,468	343	15	111	282
ZK611-6	121	172	32,165	172	−11	36	493
ZK611-7	140	267	13,369	105	−4	103	310
ZK611-8	155	211	32,365	279	−7	42	335
ZK611-9	170	347	26,007	169	−5	33	145
ZK611-10	191	110	27,874	161	0	20	337
ZK611-11	211	301	31,707	234	8	51	484
ZK611-12	230	1318	9446	540	30	145	1559
ZK611-13	251	388	1521	142	230	96	471
ZK611-14	263	171	23,933	148	5	27	266
ZK611-15	272	97	17,140	115	−10	16	170
ZK611-16	281	30	5228	185	114	46	935
ZK611-17	288	73	7622	56	8	44	155
ZK611-18	300	98	−2875	50	−8	−13	92
ZK611-19	311	276	−2485	63	10	275	485
ZK611-20	320	34	3996	47	2	36	82
ZK611-21	329	121	393	78	1	13	131
ZK611-22	341	64	−14,471	38	−3	70	52
ZK611-23	350	1246	9843	208	7	99	312
ZK611-24	362	8275	9881	743	32	−3	1418
ZK611-25	371	341	−6853	135	−1	25	106
ZK611-26	379	375	−15,549	58	13	31	171
ZK611-27	388	121	−11,722	69	71	88	369
ZK611-28	400	81	−11,241	0	15	65	172
ZK611-29	413	12,535	29,735	6409	60	80	11,126
ZK611-30	421	2456	−1434	2070	−10	−50	1290
ZK611-31	430	5466	690	4988	−10	−53	2286
ZK611-32	440	6229	−11,849	3556	−5	−39	1860
ZK611-33	449	2083	−18,142	1855	−9	−49	917
ZK611-34	458	8747	23,952	5831	−5	38	3241
ZK611-35	470	17,525	28,182	18,538	30	23	7763
ZK611-36	473	7388	5443	7033	−4	−2	2332
ZK611-37	479	5807	12,947	5843	−10	−5	1768
ZK611-38	483	8898	17,582	7139	−8	−6	4237
ZK611-39	488	3980	3816	1192	−8	14	384
ZK611-40	494	4801	14,625	1181	−6	83	766
ZK611-41	500	4247	−619	182	14	3510	681
ZK611-42	506	11,794	17,360	121	430	3149	1458
ZK611-43	512	1256	−850	−9	145	479	272
ZK611-44	518	25,885	5471	333	1624	11,880	4824
ZK611-45	521	6356	13,345	195	161	4014	1294
ZK611-46	527	15,136	−814	497	222	12,295	3196
ZK611-47	530	13,699	−3753	1326	340	5408	6965
ZK611-48	536	33,899	28,282	1524	394	58,195	8534
ZK611-49	541	49,687	35,774	2193	523	58,854	10,575
ZK611-50	545	46,070	4395	1134	49,325	77,420	29,248
ZK611-51	551	14,657	776	312	2624	6277	4050
ZK611-52	560	10,887	−10,873	190	738	2821	3315
ZK611-53	572	15,812	−8081	614	5999	7265	32,376
ZK611-54	581	10,667	−5390	519	2602	12,145	4516
ZK611-55	590	1204	5532	1823	23	227	2080
ZK611-56	604	1661	4372	198	30	159	273

Note: positive numbers indicate element influx in the system, and negative numbers indicate element efflux.

5. Discussion

5.1. Correlation of Element Migration in Different Layers

In order to explore the correlation between different elemental migration in different layers and identify the elements related to the enrichment of the main ore-forming element Cu, Pearson's correlation coefficient was applied in the study. As shown in Figure 3, the lithology of the first layer is andesite tuff. In terms of a positive correlation, the positive correlation between ΔZn and ΔS is the highest. The correlation coefficient is the largest ($R = 0.91$), followed by that between ΔAg and ΔS , $R = 0.87$. That between ΔPb and ΔS is the third-highest, $R = 0.76$, and with regard to the negative correlation, the negative correlation between ΔFe and ΔPb is the highest, and the correlation coefficient is the smallest ($R = -0.40$). This is followed by that between ΔFe and ΔAg , $R = -0.37$. Third is that between ΔFe and ΔZn , $R = -0.30$ (Figure 3a). This indicates that, in andesite tuff, the greater the migration quantity of S, the greater that of Zn, and the greater the migration quantity of Fe, the smaller that of Pb. The lithology of the second layer is andesite. Regarding the positive correlation, the positive correlation is the highest between ΔCu and ΔS . Their correlation coefficient is the largest ($R = 0.97$), followed by the positive correlation between ΔCu and ΔAg , $R = 0.87$. Third is that between ΔS and ΔAg , $R = 0.80$; regarding the negative correlation, the negative correlation between ΔCu and ΔZn is the highest, and their correlation coefficient is the smallest ($R = -0.24$), followed by that between ΔS and ΔZn , $R = -0.21$ (Figure 3b). The above results show that in andesite, when the migration quantity of S is greater, the migration quantity of Cu is greater. When the migration quantity of Zn is larger, the migration quantity of Cu is smaller. The lithology of the third layer is chalcopyritized andesite. All of the six elements show a positive correlation with each other, but the degree of correlation is different. The highest is the correlation between ΔPb and ΔAg , $R = 0.94$. Second is that between ΔS and ΔCu , $R = 0.90$. Third is that between ΔS and ΔAg , $R = 0.85$ (Figure 3c), which reveals that the enrichment of Pb is closely related to the enrichment of Ag, and the migration quantity of S is crucial to the migration quantity of Cu in chalcopyritized andesite. Fourth is altered andesite. Most of the elements in this layer show a positive correlation with each other. The correlation between ΔS and ΔZn is the highest, $R = 0.92$. The one between ΔS and ΔCu is the second-highest, $R = 0.82$. That between ΔCu and ΔZn is the third-highest, $R = 0.77$ (Figure 3d), which shows that S influx is closely related to the influx of Cu and Zn, and the enrichment of Zn promotes the enrichment of Cu. From another point of view, Cu's enrichment, as the major ore-forming element, significantly drives the enrichment of the associated ore-forming element Zn. The fifth layer is sandstone. The correlation between the six elements shows a trend of polarization. For Cu, only ΔS and ΔPb have an extremely significant negative correlation with ΔCu , and the other elements have an extremely significant positive correlation (Figure 3e). We combined all the samples and found that (Figure 3f) the positive correlation between ΔS and ΔZn is the highest, $R = 0.89$, and that between ΔS and ΔAg is the second-highest, $R = 0.70$. The above consequences indicate that the influx of S is the most supportive of Zn enrichment, followed by Ag. For Cu, ΔFe has the highest positive correlation, suggesting that Fe may be the best-associated ore-forming element.

5.2. Balance of S-Cu-(Fe, Pb, Zn, and Ag)

The relationship between the S concentration, Cu concentration, and other associated ore-forming elements' (Fe, Pb, Zn, and Ag) concentrations can be seen in Figure 4, and there is a close relationship between the three. Because there are three variables in each subgraph, concentrations of S, Fe, and Cu are three variables in Figure 4a; concentrations of S, Pb, and Cu are three variables in Figure 4b; concentrations of S, Zn, and Cu are three variables in Figure 4c; and concentrations of S, Ag, and Cu are three variables in Figure 4d. In order to display the distribution of three variables and determine the concentration of the other two elements when the Cu concentration is the highest, Figure 4 was drawn using OriginPro 2024b Software (OriginLab Corp., Northampton, MA, USA).

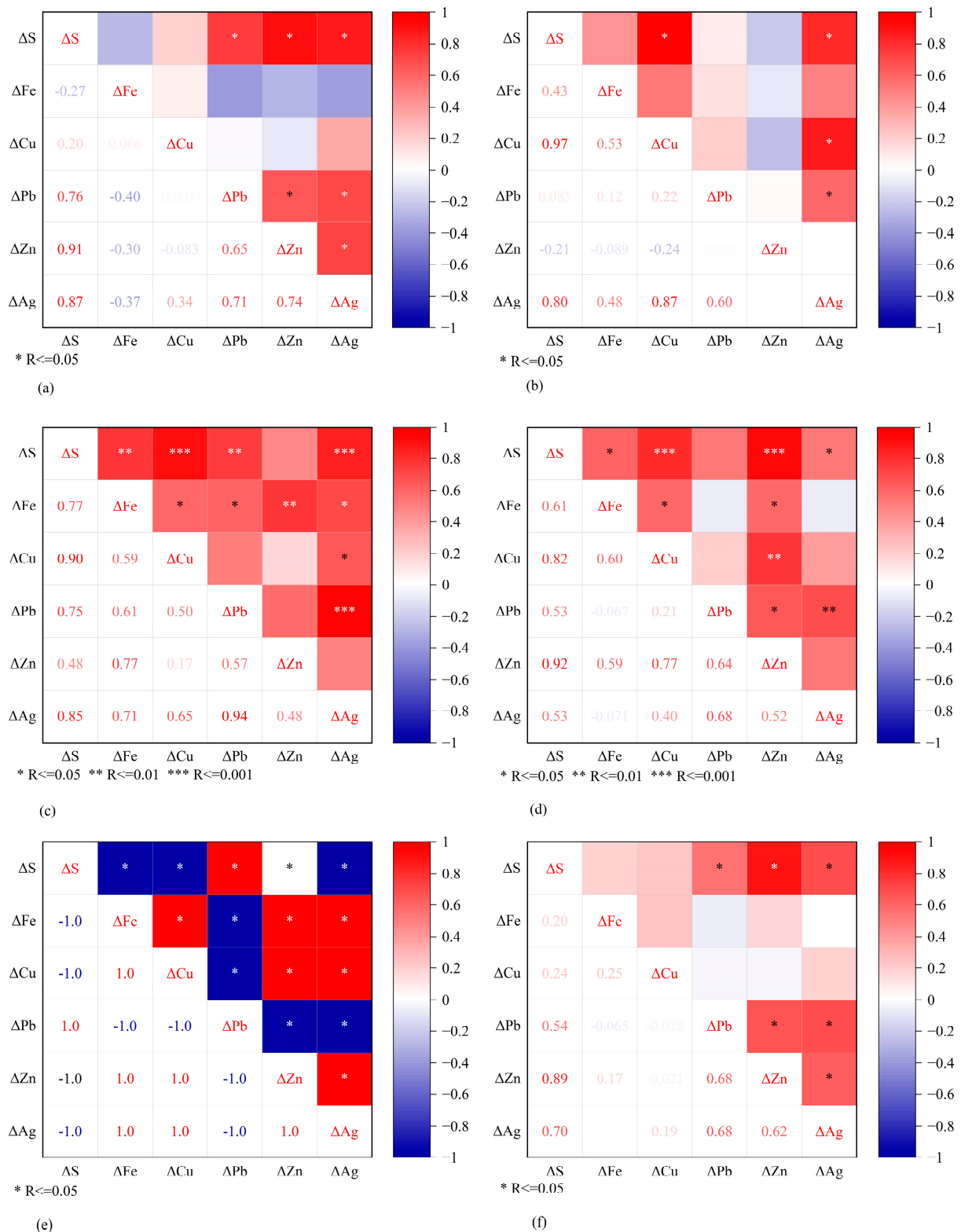


Figure 3. Pearson correlation coefficient of elemental migration. (a) The correlation between the six elements' migration in andesite tuff (1st layer); (b) the correlation between the six elements' migration in andesite (2nd layer); (c) the correlation between the six elements' migration in chalcoprytized andesite (3rd layer); (d) the correlation between the six elements' migration in altered andesite (4th layer); (e) the correlation between the six elements' migration in sandstone (5th layer); (f) the correlation between the six elements' migration in all samples.

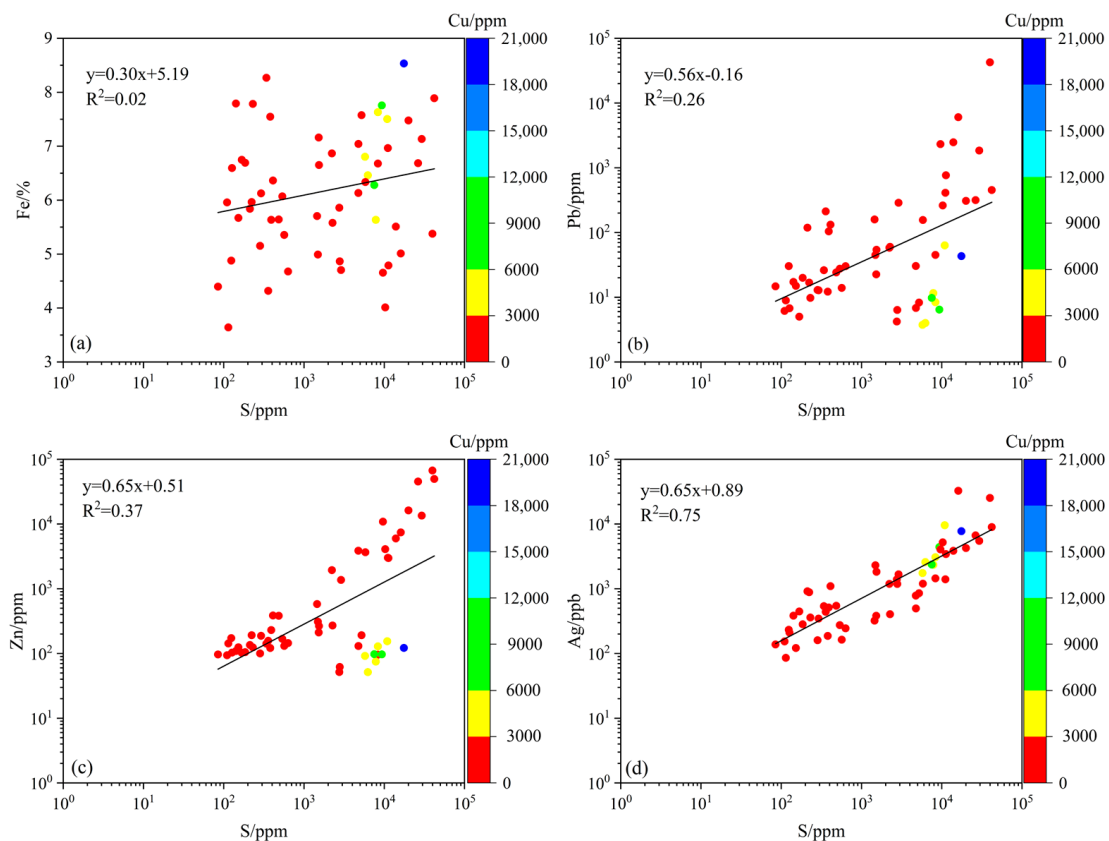


Figure 4. The distribution of the analyses in coordinates: S (ppm)—Fe (wt.%) (a); S (ppm)—Pb (ppm) (b), S (ppm)—Zn (ppm) (c); S (ppm)—Ag (ppb) (d). The different colors of the circles in the graphs correspond to the different Cu concentrations shown in a color scale on the right side of the graphs.

When S is in a relatively low concentration (<10,000 ppm), there is no significant correlation between Cu and Fe concentrations (Figure 4a). For instance, when the S concentration is ca. 100 ppm, the Fe concentration rises from 4 wt.% to 8 wt.%, and the Cu concentration does not increase significantly. It is always below 3000 ppm. When the S concentration is around 10,000 ppm, the increase in the Fe concentration will lead to a significant increase in the concentration of Cu. In contrast, the S concentration is higher than 10,000 ppm; this trend disappears again, indicating that in this study, when the S concentration is only around 10,000 ppm, the concentration of Cu will increase significantly, and the increase in the Fe concentration will maximize the enrichment of Cu. This rule also applies to the S-Cu-Pb system (Figure 4b). When the concentration of S is only about 10,000 ppm, a small increase in the Pb concentration (from 1 ppm to 100 ppm) will contribute to a substantial increase in the Cu concentration. On the other hand, when Cu is in a constant low concentration (<3000 ppm), when the S concentration increases from 100 ppm to 100,000 ppm, the Pb concentration will also increase from 10 ppm to 100,000 ppm. In terms of the S-Cu-Zn system (Figure 4c), when the S concentration is only about 10,000 ppm, the Zn concentration increases slightly near 100 ppm, and the Cu concentration will increase significantly, from 3000–6000 ppm to 18,000–21,000 ppm. In other words, the Cu concentration is most sensitive in such a condition that the S concentration is about 10,000 ppm and the Zn concentration is approximately 100 ppm. Similarly, when the Cu concentration is continuously below 3000 ppm, the S concentration increases from 100 ppm to 100,000 ppm, resulting in the Zn concentration also increasing from 100 ppm to 100,000 ppm. With regard to the S-Cu-Ag system (Figure 4d), when the S concentration is only about 10,000 ppm, and the Ag concentration rises from 1000 ppm to 10,000 ppm, under such a condition, Cu shows a substantial increase in concentration. Similarly, when

the Cu concentration is below 3000 ppm, S shows a significant positive correlation with Ag in the concentration range from 100 ppm to 100,000 ppm.

In conclusion, in terms of mineralization and Cu as the major ore-forming element, the higher the concentration of copper, the better. The above four systems have their own optimal concentration ranges for Cu, and the optimal concentration range for the S-Cu-Fe system (Figure 4a) is that the S concentration is near 10,000 ppm, and the Fe concentration is about 5.5–8.5 wt.%. The optimal concentration range of the S-Cu-Pb system (Figure 4b) is that the S concentration is near 10,000 ppm, and the Pb concentration is about 1–100 ppm. For the S-Cu-Zn system (Figure 4c), the optimal concentration range is that the S concentration is around 10,000 ppm, and the Zn concentration is around 100 ppm. For the S-Cu-Ag system (Figure 4d), the optimal concentration range is that the S concentration is around 10,000 ppm, and the Ag concentration is around 1000–10,000 ppm. It is not difficult to recognize that no matter what kind of system above, for Cu, the optimal metallogenic concentration of S is always near the order of magnitude of 10,000 ppm.

Without considering the Cu concentration, a linear correlation analysis between the S concentration and Fe, Pb, Zn, and Ag of the samples was conducted. The results showed that the correlation between S and Ag was the most significant (coefficient of determination $R^2 = 0.75$). At the same time, it was the weakest between S and Fe (coefficient of determination $R^2 = 0.02$). The coefficient of determination R^2 of S-Pb is 0.26, and the coefficient of determination R^2 of S-Zn is 0.37. The massive influx of S could lead to an abundant influx of Ag, Pb, and Zn but not to a great influx of Fe.

5.3. Evaluating the Potential of Deep Metallogeny

The SMMR of S with Cu+Fe in chalcopyrite is 35:65, about 1:2. In the main copper-mineralized section of the ZK611 drill hole (400–494 m), the main ore-forming mineral is chalcopyrite, where the average S influx is 7160 g/t, 5469 g/t for Cu, and 8796 g/t for Fe. This essentially corresponds to the SMMR of S with Cu+Fe in chalcopyrite. Based on the test results in the known copper mineralized sections, in the sections of 491–581 m with the maximum S influx, there should be stronger mineralization. However, when logging in drill cores, we found no valuable ore signs except weak copper mineralization.

The common sense explanation is that the large S influx and no mineralization of other ore-forming elements may indicate Fe influx and pyrite formation. In fact, the influx of Fe in this section is relatively great (5359 g/t), and pyritization is widespread, partly validating the above interpretation. However, although S can combine with Cu (652 g/t) and Fe (5359 g/t) to form chalcopyrite and pyrite, there remains about 13,000 g/t S which we cannot infer where it is. As this quantity of S is significant, it is thus of great significance to further investigate its occurrence; this has a critical role in understanding mineralization types, guiding the comprehensive exploration and utilization of resources, and prospecting direction.

The large influx of S generally indicates once-strong hydrothermal activities or even mineralization, signaling a prospecting promise. The issue we should first address is in which minerals the approximately 13,000 g/t of S is hosted. The first step to solve this problem is to start with the element SMMR. Rock measurements and element migration quantity of drill hole ZK611 (Table 4) indicate that, in the section at a depth of 491–581 m, Pb, Zn, and Ag all exhibit significant influx. The average influx of Pb is 4653 g/t and 18,836 g/t for Zn, with a large influx of Ag and Cd. If S combines with Pb and Zn in the system to form common Pb and Zn sulfide minerals of galena and sphalerite, based on Pb and Zn influx and the SMMR of S with Pb and Zn (based on 1 t altered rocks), about 720 g of S is needed to combine with 4653 g of Pb, and 9400 g of S to combine with 18,836 g of Zn, plus the influx of Ag and Cd. This S influx generally agrees with that of polymetallic metallogenic elements and is consistent with the overall SMMR of S with metal elements in metal sulfide minerals. It is thus inferred that there is Pb-Zn-polymetallic mineralization in the section, and its mineralization intensity is much stronger than that of copper mineralization (Figure 5).

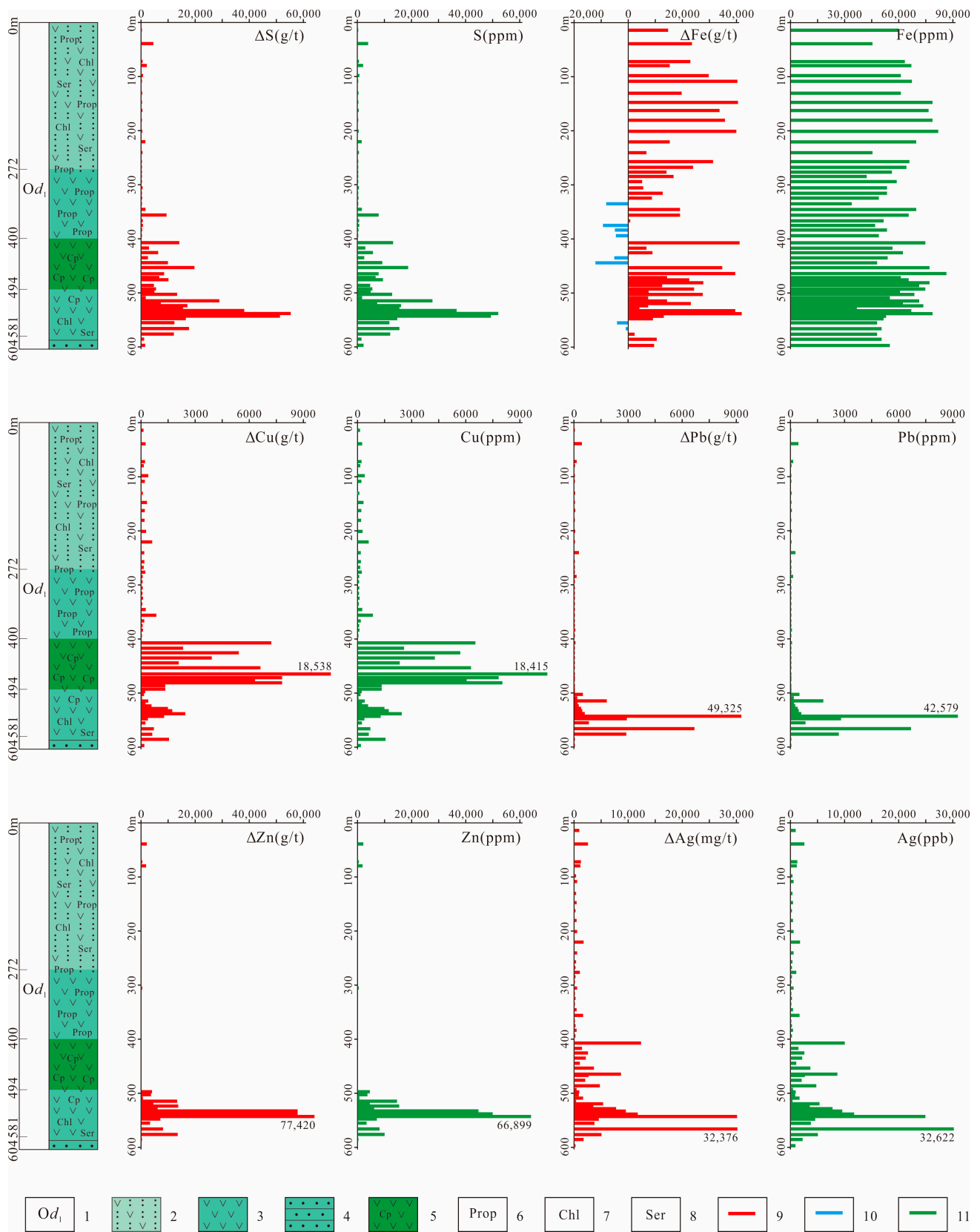


Figure 5. Bar chart of element flux and content in the ZK611 drill hole. 1—Ordovician Duobaoshan formation, 1st member; 2—Andesite tuff; 3—Andesite; 4—Sandstone; 5—Cu orebody; 6—Propylitization; 7—Chloritization; 8—Sericitization; 9—Influx; 10—Efflux; 11—Content.

In order to confirm the above speculation, we performed microscopic identification of petrographic polished sections. The result shows that there is Pb-Zn mineralization in the ZK611 drill hole at depths of 494–581 m, and the mineralization is dominated by galena and sphalerite, which display a fine granular texture (Figure 6) and cannot be identified with the naked eye. This may be the reason for no discovered Pb-Zn mineralization in the drill hole, and overall, it is a successful case of applying S anomaly using a multi-dimensional anomaly system to predict metallogenic prospects.

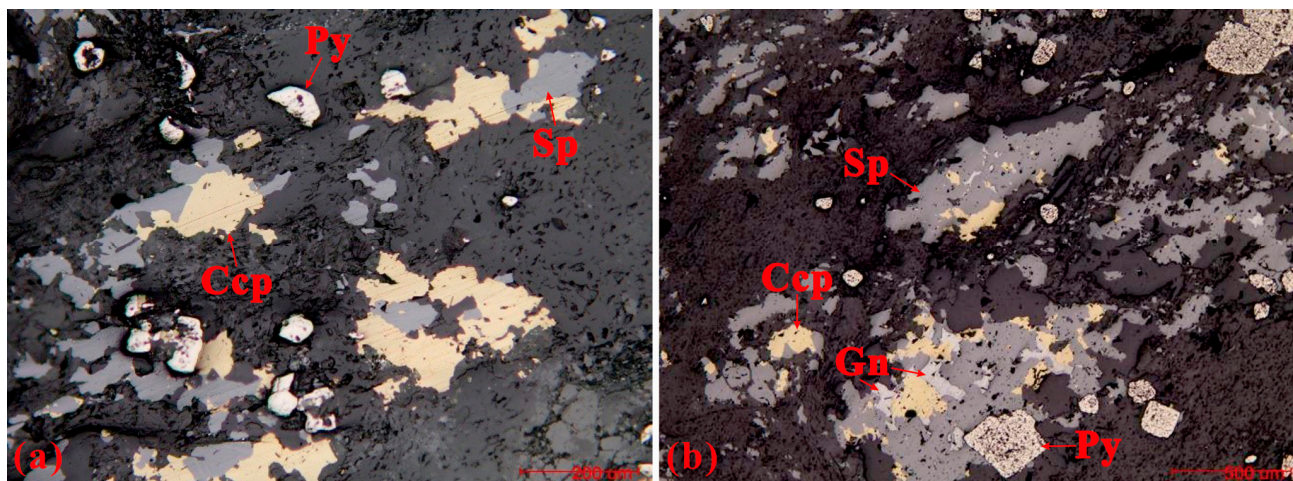


Figure 6. Optical microscopy identification. (a) No. 59 sample: 4.0% sphalerite, 1.2% chalcopyrite, 0.1% galena, and 10% pyrite. (b) No. 60 sample: 8.0% sphalerite, 1.2% chalcopyrite, 1.0% galena, and 15–20% pyrite. No. 59 and No. 60 samples were both collected from a depth of 494–581 m in the ZK611 drill hole. Abbreviations: Py = pyrite, Ccp = chalcopyrite, Sp = sphalerite, Gn = galena.

We should mention that previous prospecting work revealed two layers of noncommercial Zn orebodies with an apparent thickness of about 20 m, but their scale was much smaller than this study's. The discovery of Pb-Zn-polymetallic mineralization with an apparent thickness of 90 m indicates a new comprehensive evaluation of resources and prospecting direction, and the economic value should be further evaluated.

The element S in metal sulfides is easily oxidized and migrates with surface water, resulting in great uncertainty of a S anomaly in mineralized sections. Thus, this constrains the indication of S in the preliminary survey and prospecting stage. In the mineral exploration stage with drilling engineering, oxidation of S in drill cores is not strong and further disappears with an increasing drill depth, making it possible to use the S content to evaluate the mineralization intensity.

The application of SMMR of sulfur to metal elements in metal sulfides to predict metallogenic prospects has been preliminarily researched, and the results are encouraging. As it should be, the indication of a S anomaly is not independent, and it is only an important part of the multi-dimensional anomaly system of the geochemical system, the utilization of which will be most effective if combined with other anomaly systems. In addition, the occurrence of S is intimately associated with metallogenic environments, and the occurrence of S^{2-} and S^{6+} may contain more metallogenic information than that of a S anomaly. Relevant studies must be carried out in a systematic and orderly fashion.

6. Conclusions

1. In the orebodies, the average S influx is 7160 g/t, that of Cu is 5469 g/t, and that of Fe is 8796 g/t. In contrast, below the orebodies, the average S influx is 18,600 g/t, that of Cu is 650 g/t, and that of Fe is 5360 g/t, which disagrees with their SMMRs.
2. The element migration quantity shows that Pb's average influx is 4650 g/t, and Zn's is 18,840 g/t below the orebodies. Microscopic identification reveals that

Pb-Zn mineralization occurs in the ZK611 drill hole at a depth of 494–581 m, and the mineralization is dominated by galena and sphalerite, which display a fine granular texture.

3. The metallogenic indication of the SMMR is present in two aspects: whether mineralization stops, and the mineralization possibility in deep and peripheral areas. These two factors are critical for evaluating metallogenic prospects and achieving good results in the Tongshan copper deposit.

Author Contributions: Conceptualization, S.M.; data curation, R.L.; formal analysis, R.L.; funding acquisition, Y.L. and Z.D.; investigation, S.M. and S.T.; methodology, R.L., S.T., Z.D. and S.M.; resources, S.M.; software, R.L.; supervision, L.Z. and S.M.; writing—original draft, R.L.; writing—review and editing, Lixin Zhu and S.M. All authors have read and agreed to the published version of the manuscript.

Funding: This study is financially supported by the State Key Research and Development Plan (Grant No. 2018YFE0208300), the China Geological Survey Project (DD20242247), the Science & Technology Fundamental Resources Investigation Program (Grant No. 2022FY101800), a National Nonprofit Institute Research Grant (AS2022J11), and the Scientific Research Fund for Public Welfare from China’s Ministry of Land and Resource (Grant No. 201111008).

Data Availability Statement: Data are contained within the article.

Acknowledgments: Thanks are given to the three anonymous reviewers for their careful suggestions and to the assistant editor, for their kind assistance. We also thank the academic editors for their sincere affirmations and all those who helped with data processing.

Conflicts of Interest: The authors declare no conflicts of interest.

References

1. Cohen, D.R.; Kelley, D.L.; Anand, R.; Coker, W.B. Major advances in exploration geochemistry, 1998–2007. *Geochem.-Explor. Environ. Anal.* **2010**, *10*, 3–16. [[CrossRef](#)]
2. Yang, S.; Gong, Q.; Wen, Z.; Zhang, H.; Sun, Z.; Zhu, L.; Zhou, G.; Cheng, H.; Wang, X. Application Research of the New Technologies for Geochemical Survey. *Acta Geol. Sin.* **2011**, *85*, 1844–1877.
3. Leybourne, M.I.; Cameron, E.M. Groundwater in geochemical exploration. *Geochem. -Explor. Environ. Anal.* **2010**, *10*, 99–118. [[CrossRef](#)]
4. Piercey, S.J. An overview of petrochemistry in the regional exploration for volcanogenic massive sulphide (VMS) deposits. *Geochem.-Explor. Environ. Anal.* **2010**, *10*, 119–136. [[CrossRef](#)]
5. Caughlin, B.L. Developments in analytical technology. *Geochem.-Explor. Environ. Anal.* **2010**, *10*, 137–141. [[CrossRef](#)]
6. Grunsky, E.C. The interpretation of geochemical survey data. *Geochem.-Explor. Environ. Anal.* **2010**, *10*, 27–74. [[CrossRef](#)]
7. Jackson, R.G. Application of 3D geochemistry to mineral exploration. *Geochem.-Explor. Environ. Anal.* **2010**, *10*, 143–156. [[CrossRef](#)]
8. Coker, W.B. Future research directions in exploration geochemistry. *Geochem.-Explor. Environ. Anal.* **2010**, *10*, 75–80. [[CrossRef](#)]
9. Xu, M.Z.; Zhu, L.X.; Ma, S.M.; Sun, Y.; Tang, S.X.; Lu, L. Supergene activity discipline of elements from skarn copper mine in Beishan region: Example from Huitongshan copper mine. *J. Jilin Univ. (Earth Sci. Ed.)* **2011**, *41*, 1056–1066.
10. Zhang, Y.; Fu, S.T.; Hua, L.B.; Zhao, P.S.; Wang, B.F. Enrichment and Depletion Regularities of Trace Elements in Pb-Zn Deposits: Examples from the Dingjiashan Pb-Zn Mine in Fujian Province and Ganjiagang Pb-Zn Mine in Jiangsu Province. *Geol. Explor.* **2014**, *50*, 1126–1136. [[CrossRef](#)]
11. Zhang, D.; Zhu, L.X.; Su, L.; Ma, S.M.; Chen, H.Q.; Li, J.Y. Study on Multiple Attributes Geochemical Abnormal in Wulonggou Gold Deposit, Qinghai Province. *Acta Geol. Sin.* **2016**, *90*, 2874–2886.
12. Xi, M.J.; Ai, J.B.; Ma, S.M.; Zhu, L.X. The Genesis and Metallogenic Pattern of the Matou Mo-Cu Deposit in Chizhou District, Anhui Province, China. *Acta Geol. Sin.* **2016**, *90*, 2412–2426.
13. Wang, J.; Zhu, L.X.; Ma, S.M.; Tang, S.X.; Zhang, L.L.; Zhou, W.W. Application of the multi-attribute anomaly model for prospecting potential at depth: A case study of the Haiyu Au deposit in the Jiadong Gold Province, China. *J. Geochem. Explor.* **2019**, *207*, 106359. [[CrossRef](#)]
14. Liu, Y.P.; Zhu, L.X.; Ma, S.M.; Guo, F.S.; Gong, Q.L.; Tang, S.X.; Gopalakrishnan, G.; Zhou, Y.Z. Constraining the distribution of elements and their controlling factors in the Zhaojikou Pb-Zn ore deposit, SE China, via fractal and compositional data analysis. *Appl. Geochem.* **2019**, *108*, 104379. [[CrossRef](#)]
15. Ma, S.M.; Zhu, L.X.; Xi, M.J.; Tang, S.X. *Multidimensional Anomaly System and Its Formation Mechanism-Basic Criteria for Mineral Geochemical Exploration*; Geological Publishing House: Beijing, China, 2022; pp. 145–151.
16. Taylor, S. Abundance of chemical elements in the continental crust: A new table. *Geochim. Cosmochim. Acta* **1964**, *28*, 1273–1285. [[CrossRef](#)]

17. Hedenquist, J.W.; Simmons, S.F.; Giggenbach, W.F.; Eldridge, C.S. White Island, New Zealand, volcanic-hydrothermal system represents the geochemical environment of high-sulfidation Cu and Au ore deposition. *Geology* **1993**, *21*, 731–734. [[CrossRef](#)]
18. Seo, J.H.; Guillong, M.; Heinrich, C.A. The role of sulfur in the formation of magmatic-hydrothermal copper-gold deposits. *Earth Planet. Sci. Lett.* **2009**, *282*, 323–328. [[CrossRef](#)]
19. Liu, Y.J.; Cao, L.M.; Li, Z.L.; Wang, H.N.; Chu, T.Q.; Zhang, J.R. *Element Geochemistry*; Geological Publishing House: Beijing, China, 1984; pp. 458–470.
20. Cifuentes, G.R.; Jiménez-Millán, J.; Quevedo, C.P.; Jiménez-Espinosa, R. Transformation of S-Bearing Minerals in Organic Matter-Rich Sediments from a Saline Lake with Hydrothermal Inputs. *Minerals* **2020**, *10*, 525. [[CrossRef](#)]
21. Liu, Y.D.; Zeng, A.H.; Chen, W.J.; Cao, Y.T. The Sulfur Isotopic Characteristics of Evaporites in the Yarkand Basin of Xinjiang Province in the Paleocene and Its Paleoenvironmental Evolution. *Minerals* **2023**, *13*, 816. [[CrossRef](#)]
22. Lu, Q.F.; Qin, S.J.; Wang, W.F.; Wu, S.H.; Shao, F.J. Mineralogy and Geochemistry of High-Sulfur Coals from the M8 Coal Seam, Shihao Mine, Songzao Coalfield, Chongqing, Southwestern China. *Minerals* **2024**, *14*, 95. [[CrossRef](#)]
23. Knobloch, M.; Lottermoser, B.G. Infrared Thermography: A Method to Visualise and Analyse Sulphide Oxidation. *Minerals* **2020**, *10*, 933. [[CrossRef](#)]
24. Pokrovski, G.S.; Borisova, A.Y.; Harrichoury, J.C. The effect of sulfur on vapor-liquid fractionation of metals in hydrothermal systems. *Earth Planet. Sci. Lett.* **2008**, *266*, 345–362. [[CrossRef](#)]
25. Simon, A.C.; Ripley, E.M. The Role of Magmatic Sulfur in the Formation of Ore Deposits. In *Sulfur in Magmas and Melts: Its Importance for Natural and Technical Processes*; Behrens, H., Webster, J.D., Eds.; Reviews in Mineralogy & Geochemistry; De Gruyter: Berlin, Germany, 2011; Volume 73, pp. 513–578.
26. Yang, X.M. Sulphur Solubility in Felsic Magmas: Implications for Genesis of Intrusion-related Gold Mineralization. *Geosci. Can.* **2012**, *39*, 17–32.
27. Seo, J.H. Hydrothermal sulfur geochemistry on molybdenite deposition of the Questa Mo-deposit, New Mexico, USA. *Geosci. J.* **2014**, *18*, 419–425. [[CrossRef](#)]
28. Richards, J.P. The oxidation state, and sulfur and Cu contents of arc magmas: Implications for metallogeny. *Lithos* **2015**, *233*, 27–45. [[CrossRef](#)]
29. Kokh, M.A.; Lopez, M.; Gisquet, P.; Lanzanova, A.; Candaudap, F.; Besson, P.; Pokrovski, G.S. Combined effect of carbon dioxide and sulfur on vapor-liquid partitioning of metals in hydrothermal systems. *Geochim. Cosmochim. Acta* **2016**, *187*, 311–333. [[CrossRef](#)]
30. Hao, Y.-J.; Ren, Y.-S.; Duan, M.-X.; Tong, K.-Y.; Chen, C.; Yang, Q.; Li, C. Metallogenic events and tectonic setting of the Duobaoshan ore field in Heilongjiang Province, NE China. *J. Asian Earth Sci.* **2015**, *97*, 442–458. [[CrossRef](#)]
31. Chu, S.; Liu, J.; Xu, J.; Wei, H.; Chai, H.; Tong, K. Zircon U-Pb dating, petrogenesis and tectonic significance of the granodiorite in the Sankuanggou skarn Fe-Cu deposit, Heilongjiang Province. *Acta Petrol. Sin.* **2012**, *28*, 433–450.
32. Cai, W.-y.; Wang, K.-y.; Li, J.; Fu, L.-j.; Lai, C.-k.; Liu, H.-l. Geology, geochronology and geochemistry of large Duobaoshan Cu-Mo-Au orefield in NE China: Magma genesis and regional tectonic implications. *Geosci. Front.* **2021**, *12*, 265–292. [[CrossRef](#)]
33. Xiao, W.J.; Windley, B.F.; Hao, J.; Zhai, M.G. Accretion leading to collision and the Permian Solonker suture, Inner Mongolia, China: Termination of the central Asian orogenic belt. *Tectonics*. **2003**, *22*, 1–8. [[CrossRef](#)]
34. Li, J.Y. Permian geodynamic setting of Northeast China and adjacent regions: Closure of the Paleo-Asian Ocean and subduction of the Paleo-Pacific Plate. *J. Asian Earth Sci.* **2006**, *26*, 207–224. [[CrossRef](#)]
35. Wu, F.Y.; Sun, D.Y.; Ge, W.C.; Zhang, Y.B.; Grant, M.L.; Wilde, S.A.; Jahn, B.M. Geochronology of the Phanerozoic granitoids in northeastern China. *J. Asian Earth Sci.* **2011**, *41*, 1–30. [[CrossRef](#)]
36. Wu, G.; Chen, Y.C.; Chen, Y.J.; Zeng, Q.T. Zircon U-Pb ages of the metamorphic supracrustal rocks of the Xinghuadukou Group and granitic complexes in the Argun massif of the northern Great Hinggan Range, NE China, and their tectonic implications. *J. Asian Earth Sci.* **2012**, *49*, 214–233. [[CrossRef](#)]
37. Zeng, Q.-D.; Liu, J.-M.; Chu, S.-X.; Wang, Y.-B.; Sun, Y.; Duan, X.-X.; Zhou, L.-L.; Qu, W.-J. Re-Os and U-Pb geochronology of the Duobaoshan porphyry Cu-Mo-(Au) deposit, northeast China, and its geological significance. *J. Asian Earth Sci.* **2014**, *79*, 895–909. [[CrossRef](#)]
38. Ge, W.C.; Wu, F.Y.; Zhou, C.Y.; Rahman, A.A.A. Emplacement age of the Tahe granite and its constraints on the tectonic nature of the Ergun block in the northern part of the Da Hinggan Range. *Chin. Sci. Bull.* **2005**, *50*, 2097–2105. [[CrossRef](#)]
39. She, H.Q.; Li, J.W.; Xiang, A.P.; Guan, J.D.; Yang, Y.C.; Zhang, D.Q.; Tan, G.; Zhang, B. U-Pb ages of the zircons from primary rocks in middle-northern Daxinganling and its implications to geotectonic evolution. *Acta Petrol. Sin.* **2012**, *28*, 571–594.
40. Li, L.Y.; Zhang, C.H.; Feng, Z.Q. The Ordovician Arc-Basin System in the Northern Great Xing’an Range (Northeast China): Constraints from Provenance Analysis of the Luohe Formation. *Minerals* **2024**, *14*, 258. [[CrossRef](#)]
41. Seltmann, R.; Porter, T.M.; Pirajno, F. Geodynamics and metallogeny of the central Eurasian porphyry and related epithermal mineral systems: A review. *J. Asian Earth Sci.* **2014**, *79*, 810–841. [[CrossRef](#)]
42. Ge, W.C.; Wu, F.Y.; Zhou, C.Y.; Zhang, J.H. Porphyry Cu-Mo deposits in the eastern Xing’an-Mongolian Orogenic Belt: Mineralization ages and their geodynamic implications. *Chin. Sci. Bull.* **2007**, *52*, 3416–3427. [[CrossRef](#)]
43. Wang, J.; Hattori, K.; Yang, Y.C.; Yuan, H.Q. Zircon Chemistry and Oxidation State of Magmas for the Duobaoshan-Tongshan Ore-Bearing Intrusions in the Northeastern Central Asian Orogenic Belt, NE China. *Minerals* **2021**, *11*, 503. [[CrossRef](#)]

44. Zhao, Z.H.; Qiao, K.; Liu, Y.W.; Chen, J.; Li, C.L. Geochemical Data Mining by Integrated Multivariate Component Data Analysis: The Heilongjiang Duobaoshan Area (China) Case Study. *Minerals* **2022**, *12*, 1035. [[CrossRef](#)]
45. Zhao, Z.H.; Chen, J.; Cheng, B.B.; Liu, Y.W.; Qiao, K.; Cui, X.M.; Yin, Y.C.; Li, C.L. Spatial Analysis of Structure and Metal Mineralization Based on Fractal Theory and Fry Analysis: A Case Study in Nenjiang-Heihe Metallogenic Belt. *Minerals* **2023**, *13*, 313. [[CrossRef](#)]
46. Zhao, Y.Y.; Ma, Z.H.; Zhong, C.X. Geochemistry and its model of prospecting of Tongshan copper deposit, Heilongjiang Province. *Geol. Explor.* **1995**, *31*, 48–54.
47. Zhao, Y.M.; Bi, C.S.; Zou, X.Q.; Sun, Y.L.; Du, A.D.; Zhao, Y.M. The Re-Os isotopic age of molybdenite from Duobaoshan and Tongshan porphyry copper (molybdenum) deposits. *Acta Geosci. Sin.* **1997**, *18*, 61–67.
48. Du, Q.; Chen, M.X. The genetic model of Duobaoshan porphyry copper deposit. *Miner. Depos.* **1983**, *2*, 42–48.
49. Wu, G.; Liu, J.; Zhong, W.; Zhu, M.T.; Mei, M.; Wan, Q. Fluid inclusion study of the Tongshan porphyry copper deposit, Heilongjiang Province, China. *Acta Petrol. Sin.* **2009**, *25*, 2995–3006.
50. Gresens, R.L. Composition-volume relationships of metasomatism. *Chem. Geol.* **1967**, *2*, 47–65. [[CrossRef](#)]
51. Grant, J.A. The isocon diagram—A simple solution to Gresens equation for metasomatic alteration. *Econ. Geol.* **1986**, *81*, 1976–1982. [[CrossRef](#)]
52. Grant, J.A. Isocon analysis: A brief review of the method and applications. *Phys. Chem. Earth* **2005**, *30*, 997–1004. [[CrossRef](#)]
53. Deng, H.L.; Tu, G.Z.; Li, C.Y.; Liu, C.Q. Mass balance of open geochemical systems: 1. Theory. *Acta Mineral. Sin.* **1999**, *19*, 121–131.
54. Ai, J.B.; Ma, S.M.; Fan, L.J. A quantitative discussion on element mass migration in the Wunugetushan porphyry Cu-Mo deposit, Inner Mongolia. *Acta Geosci. Sin.* **2013**, *34*, 193–202.
55. Ai, J.B.; Ma, S.M.; Zhu, L.X.; Fan, L.J.; Hu, Z.X.; Xi, M.J. Characteristic and migration regularity of major elements and REEs in Matou porphyry Mo-Cu deposit in the middle-lower reaches of Yangtze River. *Acta Geol. Sin.* **2013**, *87*, 691–702.
56. Guo, S.; Ye, K.; Chen, Y.; Liu, J.; Zhang, L. Introduction of mass-balance calculation method for component transfer during the opening of a geological system. *Acta Petrol. Sin.* **2013**, *29*, 1486–1498.
57. Maclean, W.H.; Kranidiotis, P. Immobile elements as Monitors of mass-transfer in hydrothermal alteration-Phelps Dodge massive sulfide deposit, Matagami, Quebec. *Econ. Geol.* **1987**, *82*, 951–962. [[CrossRef](#)]
58. Ellahi, S.S.; Taghipour, B.; Zarasvandi, A.; Bird, M.I.; Somarin, A.K. Mineralogy, Geochemistry and Stable Isotope Studies of the Dopolan Bauxite Deposit, Zagros Mountain, Iran. *Minerals* **2016**, *6*, 11. [[CrossRef](#)]
59. Reinhardt, N.; Proenza, J.A.; Villanova-de-Benavent, C.; Aiglsperger, T.; Bover-Arnal, T.; Torró, L.; Salas, R.; Dziggel, A. Geochemistry and Mineralogy of Rare Earth Elements (REE) in Bauxitic Ores of the Catalan Coastal Range, NE Spain. *Minerals* **2018**, *8*, 562. [[CrossRef](#)]
60. Li, C.; Li, Z.L.; Wu, T.; Luo, Y.Q.; Zhao, J.; Li, X.R.; Yang, W.C.; Chen, X.G. Metallogenic Characteristics and Formation Mechanism of Naomugeng Clay-Type Lithium Deposit in Central Inner Mongolia, China. *Minerals* **2021**, *11*, 238. [[CrossRef](#)]
61. Yan, M.C.; Chi, Q.H. *The Chemical Compositions Crust and Rocks in the Eastern Part of China*; Science House: Beijing, China, 1997; pp. 106–107.

Disclaimer/Publisher’s Note: The statements, opinions and data contained in all publications are solely those of the individual author(s) and contributor(s) and not of MDPI and/or the editor(s). MDPI and/or the editor(s) disclaim responsibility for any injury to people or property resulting from any ideas, methods, instructions or products referred to in the content.